PNAS RESEARCH ARTICLE | IMMUNOLOGY AND INFLAMMATION

Regulatory T cells play a crucial role in maintaining sperm tolerance and male fertility

Ferran Barrachina[a], Kiera Ottino[a], Maia Lina Elizagaray[a], Maria Gracia Gervasi[b,c,1], Leona J. Tu[a], Styliani Markoulaki[c,2], Raul G. Spallanzani[d,3], Diane Capen[a], Dennis Brown[a], and Maria Agustina Battistone[a,4]

Edited by Jeffrey Bluestone, Sonoma Biotherapeutics, San Francisco, CA 94080; received April 27, 2023; accepted July 31, 2023

Regulatory T cells (Tregs) modulate tissue homeostatic processes and immune responses. Understanding tissue-Treg biology will contribute to developing precision-targeting treatment strategies. Here, we show that Tregs maintain the tolerogenic state of the testis and epididymis, where sperm are produced and mature. We found that Treg depletion induces severe autoimmune orchitis and epididymitis, manifested by an exacerbated immune cell infiltration [CD4 T cells, monocytes, and mononuclear phagocytes (MPs)] and the development of antisperm antibodies (ASA). In Treg-depleted mice, MPs increased projections toward the epididymal lumen as well as invading the lumen. ASA-bound sperm enhance sperm agglutination and might facilitate sperm phagocytosis. Tolerance breakdown impaired epididymal epithelial function and altered extracellular vesicle cargo, both of which play crucial roles in the acquisition of sperm fertilizing ability and subsequent embryo development. The affected mice had reduced sperm number and motility and severe fertility defects. Deciphering these immunoregulatory mechanisms may help to design new strategies to treat male infertility, as well as to identify potential targets for immunocontraception.

EVs | infertility | sperm tolerance | sperm function | inflammation

Immune tolerance is a process that allows an individual to be repeatedly exposed to the same antigen without evoking an aggressive immune response (1–4). Sperm populate the reproductive tract at puberty, long after the establishment of systemic immune tolerance; therefore, male reproductive function relies on tolerance mechanisms to the onslaught of sperm antigens, similar in principle to the mechanisms that control tolerance to food antigens and commensal bacteria in the digestive tract.

Infertility affects ~17% of couples worldwide, and male factors are involved in ~50% of these cases (5, 6), half of which are classified as idiopathic (7), highlighting our poor knowledge of male reproductive physiology. A critical, but understudied, aspect of male health is the close interaction between the reproductive and immune systems in the epididymal environment. After leaving the testis, sperms acquire motility and potential for fertilization during their transit through the epididymis (8, 9). The ability of this organ to prevent autoimmune responses against antigenic spermatozoa, while initiating immune defense against pathogens, is one of the most intriguing aspects of male reproductive biology. Thus, a finely tuned balance between sperm tolerance and immune defense is required to maintain epididymal function while protecting sperm against stressors. Breakdown of the homeostasis between the epididymal mucosa and sperm might be responsible for a significant proportion of male infertility cases (10–14). The extraordinary organization of epididymal epithelial cells and immunocytes may contribute to the establishment of a milieu that maintains the epididymal "immune-privileged" environment.

Maintaining peripheral tolerance to sperm in the epididymis is crucial to avoid the development of autoimmune reactions such as the production of antisperm antibodies (ASA), which cause infertility (15–18). Vasectomy is a worldwide male contraceptive approach, and over 50% of vasectomized men develop ASA (19–22). However, the mechanism of the postvasectomy autoimmune-associated response isn't well characterized. Immune tolerance involves the differentiation of naive $CD4^+$ T cells (T lymphocytes) into a subpopulation of regulatory T cells (Tregs), characterized by the expression of the transcriptional regulator forkhead box P3 (Foxp3) (2, 23). Tregs have been characterized in several nonlymphoid organs and mucosal tissue sites (3, 4). Given the canonical roles of Tregs as immune response regulators, as well as their location-specific functions, an increasing body of research demonstrates that Treg populations in mucosal tissues are crucial in both homeostasis and disease (4). It was reported that, after vasectomy, sperm tolerance depends on the interaction of exposed sperm antigens, which are released into the epididymal interstitium, with Tregs (22). Moreover, the loss of tolerance is a likely cause of autoimmune infertility. Autoimmune polyendocrine disease type I (APS-I), which is

Significance

Regulatory T cells (Tregs) are specialized immune cells that modulate tissue homeostasis. In the male reproductive tract, prevention of autoimmune responses against antigenic spermatozoa, while ensuring protection against stressors, is a key determinant of fertility. Using an autoimmunity-induced model, we uncovered the role of Tregs in maintaining the tolerogenic state of the testis and epididymis. The loss of tolerance induced an exacerbated immune cell infiltration and the development of anti-sperm antibodies, which caused severe male subfertility. By identifying immunoregulatory mechanisms in the testis and epididymis, our study may lead to the development of therapies for infertility and identifying potential targets for immunocontraception. Ultimately, such knowledge fills gaps related to reproductive mucosa, which is an understudied facet of human male health.

The authors declare no competing interest.

This article is a PNAS Direct Submission.

[1]Present address: Department of Animal Science, University of Connecticut, Storrs, CT 06269.

[2]Present address: Department of Cell and Developmental Biology, Feinberg School of Medicine, Northwestern University, Chicago, IL 60208.

[3]Present address: KSQ Therapeutic, 4 Maguire Rd, Lexington, MA 02421.

[4]To whom correspondence may be addressed. Email: mbattistone@mgh.harvard.edu.

This article contains supporting information online at https://www.pnas.org/lookup/suppl/doi:10.1073/pnas.2306797120/-/DCSupplemental.

Published September 7, 2023.

caused by mutations in the autoimmune regulator (AIRE) gene (24) and is associated with impaired Treg function, induces autoimmune orchitis and infertility (25, 26). Mice with a deletion of the *Aire* gene presented normal testicular function, but ASA were detected; the epididymal interstitial tissue contained leukocytic infiltration, and male fertility was reduced (27, 28). In addition, after 8 wk of Treg depletion, severe autoimmune orchitis was observed, characterized by testicular and epididymal tubular atrophy (19). However, that study focused on testicular damage over the long term after Treg ablation, and the epididymal phenotype was not fully characterized.

Additionally, certain autoimmune diseases, such as lupus erythematosus, rheumatoid arthritis, Type I diabetes, or various types of systemic vasculitis, including Behcet's disease, which affect the blood vessels of the testis and/or epididymis, increase the risk of male infertility. This is attributed to the detrimental effects of local inflammation in the male reproductive tract, ultimately leading to impaired fertility (29–31). Moreover, autoimmune diseases that involve hormone dysregulation could also affect male fertility, such as the autoimmune Hashimoto's thyroiditis (29).

In the current study, we show that disruption of the mechanisms driving immune tolerance unleashes pro-inflammatory responses in the epididymis, characterized by severe infiltration of subsets of mononuclear phagocytes (MPs), monocytes, and neutrophils, and the production of ASA. The autoimmune epididymitis induced low epididymal sperm counts, impaired sperm motility, low fertilization rates, and altered extracellular vesicle (EV) cargo, ultimately resulting in a severe male subfertility phenotype. Thus far, our results show that Tregs play a key role in maintaining a tolerogenic environment that protects sperm during their transit and storage in the epididymis.

Results

Regulatory T Cells (Tregs) in wild-type (WT) Murine Testis and Epididymis. We first evaluated the abundance of Tregs ($Foxp3^+CD4^+CD45^+$, Fig. 1*A*) in the epididymis of WT mice at different ages (4-, 6-, 8-, 12-, and 20-wk-old mice) by flow cytometry (Fig. 1 *B*, *i* and *ii*). We observed a decline in the Treg abundance related to aging (from 4- to 20-wk-old WT mice). This age-related reduction was much more pronounced in the distal epididymis. Importantly, spermatozoa start populating the epididymis at 4 to 6 postnatal wk. In the distal epididymis, but not in the proximal regions, we revealed a decrease of total immune cells ($CD45^+$ cells) related to aging (*SI Appendix*, Fig. S1 *A, i* and *ii*), while no significant changes in the $CD4^+$ T lymphocyte abundance were observed in either the proximal or distal epididymis (*SI Appendix*, Fig. S1 *B*, *i* and *ii*). In the testis of WT mice, the Treg population was numerically similar to that seen in the proximal epididymis, without significant differences over time (Fig. 1 *B, iii*). We revealed a decrease of total immune cells ($CD45^+$ cells) related to aging (*SI Appendix*, Fig. S1 *A, iii*), together with an age-dependent increase (from 6- to 20-wk-old mice) in the $CD4^+$ T lymphocyte abundance in the testis (*SI Appendix*, Fig. S1 *B, iii*). Instead, in the spleen, we observed that while the abundance of Tregs increases (Fig. 1 *B, iv*) with aging, the amount of CD4 T cells decreases (*SI Appendix*, Fig. S1 *B, iv*). No changes in the abundance of $CD45^+$ were observed in the spleen (*SI Appendix*, Fig. S1 *A, iv*). Moreover, in the epididymis of old mice (20-wk-old mice), we detected a decreased abundance of $CD69^+Foxp3^+CD4^+$ cells (Fig. 1*C*), indicating a reduction of epididymal Treg function. Furthermore, we found that Tregs populate the interstitium of all epididymal segments and are near a subset of MPs ($MHCII^+$ cells) and clear cells (CCs, B1 $V\text{-}ATPase^+$ cells) (Fig. 1*D*).

Breakdown of Immune Tolerance. Using transgenic mice that express the diphtheria toxin (DT) receptor (DTR) under the control of the Foxp3 promoter (Foxp3-DTR mice), we were able to disrupt tolerance by ablation of Tregs using a DT-based depletion (Fig. 2*A*). Our data showed that 3 d after DT injections, there was a reduction in the relative abundance of Tregs in the proximal and distal epididymides and in the testis of Foxp3-DTR mice (Fig. 2*B*). The reduction in Tregs caused an early infiltration of monocytes ($Ly6C^+Ly6G^-CD11b^+CD45^+$; Fig. 2*C*) and $CD4^+$ T cells ($CD4^+CD45^+$; Fig. 2*D*) in the proximal and distal epididymal segments and testis of DT-injected Foxp3-DTR mice. This early immune response did not result in an overall infiltration of other immune cells, such as $CD45^+$ cells, neutrophils ($Ly6G^+CD11b^+CD45^+$), $MHCII^+$ MPs ($MHCII^+CD11b^+CD45^+$), and $F4/80^+$ MPs ($F4/80^+Ly6G^-Ly6C^-CD11b^+CD45^+$) in the epididymis and testis of DT-injected Foxp3-DTR mice, compared to DT-injected WT mice (*SI Appendix*, Fig. S2).

Treg Depletion Resulted in Exacerbated Immune Cell Infiltration in the Epididymis. Two weeks after DT treatment, the reduction in the relative abundance of Tregs was maintained in the distal epididymis of Foxp3-DTR mice (Fig. 3 *A* and *B*), and the epididymal inflammation became more pronounced in both the proximal and distal regions. Flow cytometry analyses showed a widespread infiltration of $CD45^+$ cells in both proximal and distal epididymides of DT-injected Foxp3-DTR mice (Fig. 3*C*). Specifically, we observed infiltration of $CD4^+$ T lymphocytes (Fig. 3*D*), monocytes (Fig. 3*E*), neutrophils (Fig. 3*F*), $MHCII^+$ MPs (Fig. 3*G*), and $F4/80^+$ MPs (Fig. 3*H*). Abundant cell infiltration was observed in the interstitium and lumen of the epididymis after Treg depletion, using hematoxylin and eosin (H&E) staining (*SI Appendix*, Fig. S3). Confocal microscopy showed many $MHCII^+$ MPs (Fig. 3*I*, red) and $F4/80^+$ MPs (Fig. 3*J*, red) in all the epididymal segments of DT-injected Foxp3-DTR mice. We also saw a greater number of luminal-reaching intraepithelial projections from $F4/80^+$ MPs in the initial segments (IS) of Foxp3-DTR mice after DT treatment (Fig. 3 *J* and *K*, arrows). Surprisingly, after the depletion of Tregs, $F4/80^+$ MPs invaded the epididymal lumen to presumably eliminate aberrant spermatozoa (Fig. 3*J*; arrowheads). All these histopathological results are consistent with the flow cytometry analysis.

Consequences of Treg Depletion on Epididymal Morphology. Despite the severe epididymal immune cell infiltration 2 wk after Treg depletion, we observed no apparent damage in the epididymal epithelium using antibodies that detect epithelial cell markers: V-ATPase B1 subunit (a marker of CCs; *SI Appendix*, Fig. S4), AQP9 (a marker of principal cells; *SI Appendix*, Fig. S4), cytokeratin-5 (KRT5; a marker of basal cells; *SI Appendix*, Fig. S5), and the tight junction protein Zonula occludens-1 (ZO-1; *SI Appendix*, Fig. S5). In addition, no differences were observed in the number of apoptotic cells (cleaved caspase-3^+ cells; *SI Appendix*, Fig. S6, red) in the epididymis of DT-injected Foxp3-DTR mice versus WT. Overall, the immune response resulting from the immunotolerance loss did not produce major epithelial structure defects, which suggests that the epithelium is resistant to damage and confers protection to gametes. However, confocal microscopy revealed that epididymal CCs from DT-injected B1-EGFP Foxp3-DTR mice displayed an increased number of $EGFP^+$ CC apical protrusions (blebs; *SI Appendix*, Fig. S7, arrows), suggesting that CCs respond during this inflammatory process, in concordance with their role in immune activation against pathogens previously reported (32).

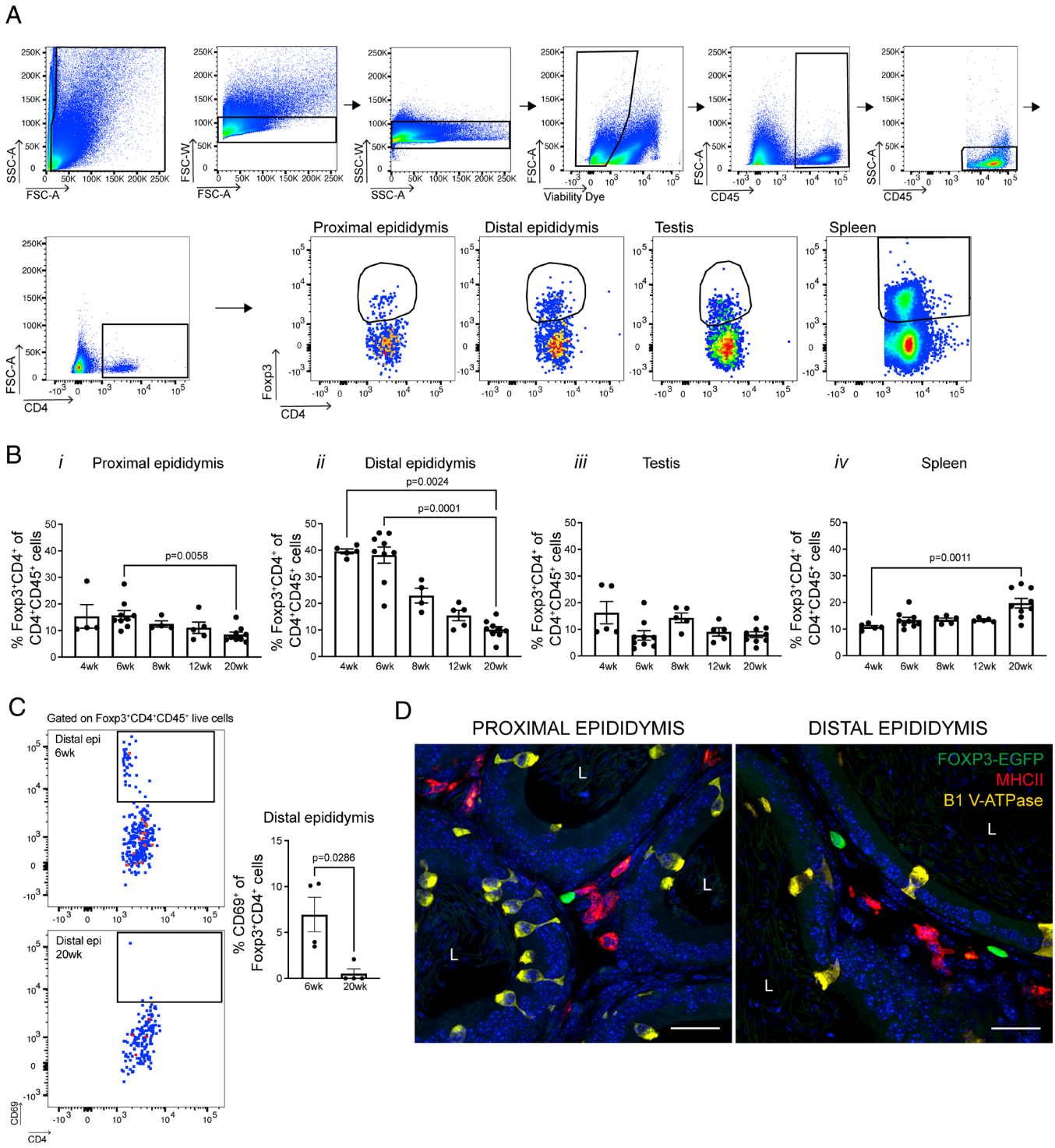

Fig. 1. Treg population throughout WT mouse lifespan. (*A*) Flow cytometry gating strategy used to study regulatory T cells (Tregs; Foxp3$^+$CD4$^+$CD45$^+$) in the proximal and distal epididymides, testis, and spleen. FSC-A: forward scatter area, SSC-A: side scatter area, FSC-W: forward scatter width. (*B*) Relative abundance of Tregs in the proximal and distal epididymides, testis, and spleen at different ages (4-, 6-, 8-, 12-, and 20-wk-old mice) by flow cytometry. (*C*) Flow cytometry analysis of CD69$^+$ Tregs in the epididymis. Each dot represents a pool of two proximal epididymides, two distal epididymides, two testes, or one spleen from each mouse. Data were analyzed using the Kruskal–Wallis test followed by Dunn's post hoc test (Fig. 1*B*), or Mann–Whitney *U* test (Fig. 1*C*). Data are shown as means ± SEM. (*D*) Confocal microscopy images showing Foxp3-EGFP$^+$ Tregs (green), clear cells (CCs; B1 V-ATPase$^+$ cells; yellow), and MHCII$^+$ MPs (red) in the proximal and distal epididymal regions of Foxp3-EGFP transgenic mice (12 wk). Nuclei are labeled with DAPI (blue). Bars: 20 μm. L: lumen.

Testicular Immune Infiltration Associated with Treg Depletion. In the testis, 2 wk after Treg depletion, we observed a similar immunological response to the epididymis. First, flow cytometry showed similar Treg relative abundance in the testis of DT-injected WT and Foxp3-DTR mice (*SI Appendix*, Fig. S8*A*). However, the early depletion of Tregs in the testis of Foxp3-DTR mice (Fig. 2 *B, ii*) resulted in a severe infiltration of CD45$^+$ cells (*SI Appendix*, Fig. S8*B*), CD4$^+$ T lymphocytes (*SI Appendix*, Fig. S8*C*), monocytes (*SI Appendix*, Fig. S8*D*), MHCII$^+$ MPs (*SI Appendix*, Fig. S8*E*), and F4/80$^+$ MPs (*SI Appendix*, Fig. S8*G*). Confocal imaging confirmed an increase in the amount of MHCII$^+$ MPs (*SI Appendix*, Fig. S8*F*, red) and F4/80$^+$ MPs

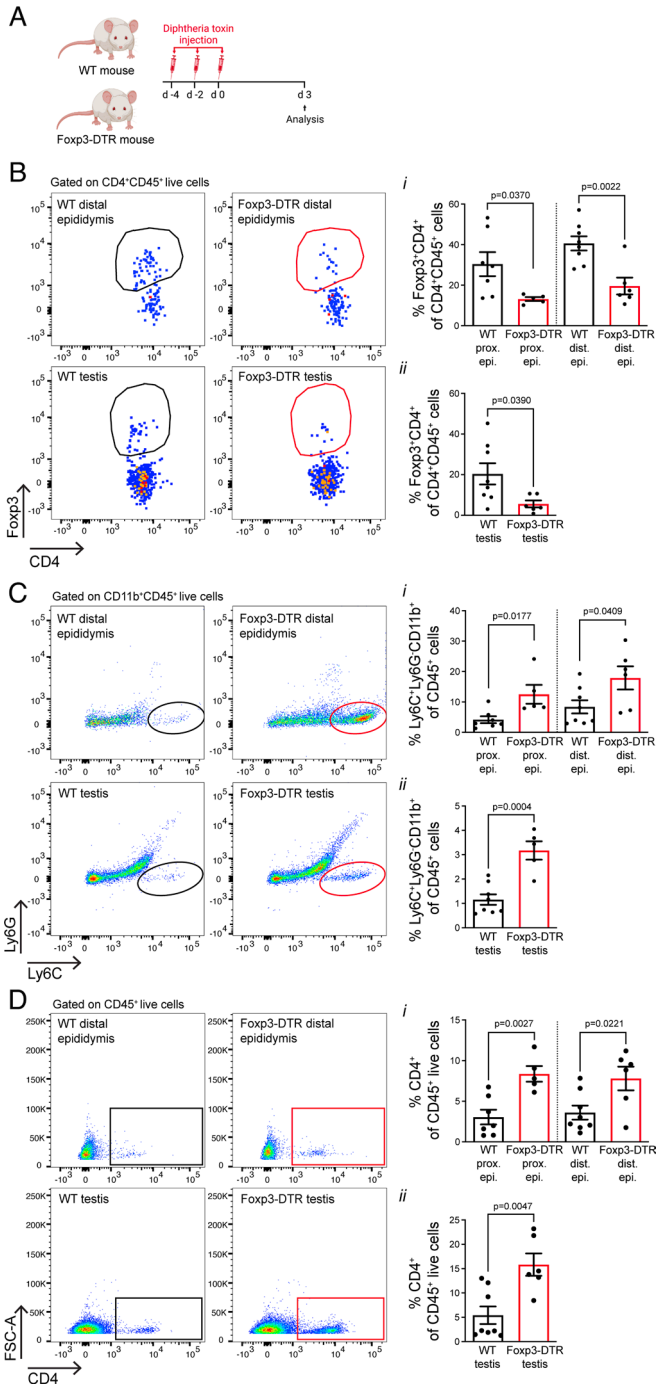

Fig. 2. Immune cell infiltration in the epididymis and testis of Foxp3-DTR mice 3 d after Treg depletion. (*A*) Treg cell depletion protocol and analysis 3 d after DT treatment. Flow cytometry analysis of the relative abundance of different immune cells in the proximal and distal epididymides and testes of WT and Foxp3-DTR mice 3 d after DT treatment: (*B*) Tregs ($Foxp3^+CD4^+CD45^+$), (*C*) monocytes ($Ly6C^+Ly6G^-CD11b^+CD45^+$), and (*D*) $CD4^+$ T lymphocytes ($CD4^+CD45^+$). Note that flow cytometry dot blot analysis for distal epididymis and testis is shown, but quantitative data for both proximal and distal as well as testicular tissues is provided. Each dot represents a pool of proximal or distal epididymides or testes from each mouse. Data were analyzed using Student's *t* test (Fig. 2 *B, i, C, i* dist., *C, ii,* and *D, i*) or Mann–Whitney *U* test (Fig. 2 *B, ii, C, i* prox., *D, ii*). Data are shown as means ± SEM.

(*SI Appendix*, Fig. S8*H*, red) into the testicular parenchyma after the depletion of Tregs, but no extravasation through the blood-testis barrier (BTB) was observed. In addition, a complete process of spermatogenesis, in which progenitor spermatogonia develops into mature spermatozoa, was observed in both groups by H&E staining (*SI Appendix*, Fig. S9*A*), indicating no impairment in sperm production in DT-injected Foxp3-DTR mice. Moreover, no differences were observed in the number of apoptotic cells (*SI Appendix*, Fig. S9*B*, red) in the testis of DT-injected Foxp3-DTR mice compared to controls.

Increased Production of Autoantibodies after Treg Depletion. Enzyme-Linked Immunosorbent Assay (ELISA) revealed that, 2 wk after DT injections, serum from Foxp3-DTR mice had increased levels of autoantibodies (IgG) against testicular, epididymal, and proximal and distal sperm antigens, compared to DT-injected WT mice (Fig. 4*A*). Confocal microscopy showed IgG accumulation in the epididymal and testicular interstitium of DT-injected Foxp3-DTR mice (Fig. 4*B*, green; see all epididymal regions in *SI Appendix*, Fig. S10). Interestingly, in the epididymal lumen of DT-injected Foxp3-DTR mice, we found agglutinated sperm containing IgG^+ antisperm antibodies (ASA) (Fig. 4 *B* and *C*, green, arrowheads). These clusters of IgG^+ ASA-bound sperm (green) were surrounded by $F4/80^+$ MPs (red) (Fig. 4*C*), potentially leading to the phagocytosis of antibody-bound sperm (Fig. 4*C*, top panel, red). Moreover, flow cytometry showed an increased abundance of Ig^+ cells (sperm) isolated from the epididymal lumen of DT-injected Foxp3-DTR mice (Fig. 4*D*). Immunofluorescence (IF) studies also revealed IgG^+ ASA (green) attached to both the head and tail of proximal and distal epididymal sperm from Treg-depleted mice (Fig. 4*E*).

Treg Depletion Resulted in Severe Immunological Male Subfertility. Computer-assisted sperm analysis (CASA) revealed low sperm counts in the proximal and the distal epididymis (Fig. 5*A*) and reduced total sperm motility (Fig. 5*B* and Movies S1 and S2) in DT-injected Foxp3-DTR mice. No differences in capacitation-associated sperm motility parameters were observed between DT-injected WT and Foxp3-DTR mice (*SI Appendix*, Table S1). In vitro fertilization (IVF), using the same sperm concentration retrieved from both groups of animals, showed a significant decrease in cleavage of oocytes to the two-cell stage in the Treg-depleted mice (Fig. 5*C*). In addition, this severe decrease in fertility was also observed in natural mating experiments. The number of pups per litter was significantly reduced when using DT-injected Foxp3-DTR male mice versus WT mice and, indeed, only two out of nine DT-injected Foxp3-DTR males had pups (Fig. 5*D*). Overall, all the inflammatory-inflicted damage that occurred after Treg depletion had a detrimental effect on epididymal sperm function, resulting in severe immunological subfertility.

Disruption of Immune Tolerance Changed Epididymal EV Protein Cargo. During its transit through the epididymis, spermatozoa undergo maturation through contact with EVs (epididymosomes) released by epididymal epithelial cells (33). Any alteration of the epididymal epithelial function could result in defects in sperm maturation, leading to impairment of the fertilization process. Thus, we characterized the protein-content profile of epididymal EVs after immune tolerance disruption by performing mass spectrometry-based label-free quantitative proteomics. EVs were obtained from the proximal and distal epididymides of WT and Foxp3-DTR mice 2 wk after DT treatment (Fig. 6*A*). Transmission electron microscopy and nanoparticle tracking analysis (NTA) showed a typical EV-like double-membrane structure with a size ranging from 50 nm to 200 nm (*SI Appendix*, Fig. S11). The proteomic analysis of EVs from proximal and distal regions of DT-injected WT and Foxp3-DTR mice resulted in the identification of 2,313 proteins (Dataset S1). Comparison of the four different EV populations demonstrated a shared proteomic signature of 643 proteins (27.8%; Fig. 6*B*). Moreover, this analysis showed that over 700 proteins were identified exclusively in EVs from WT

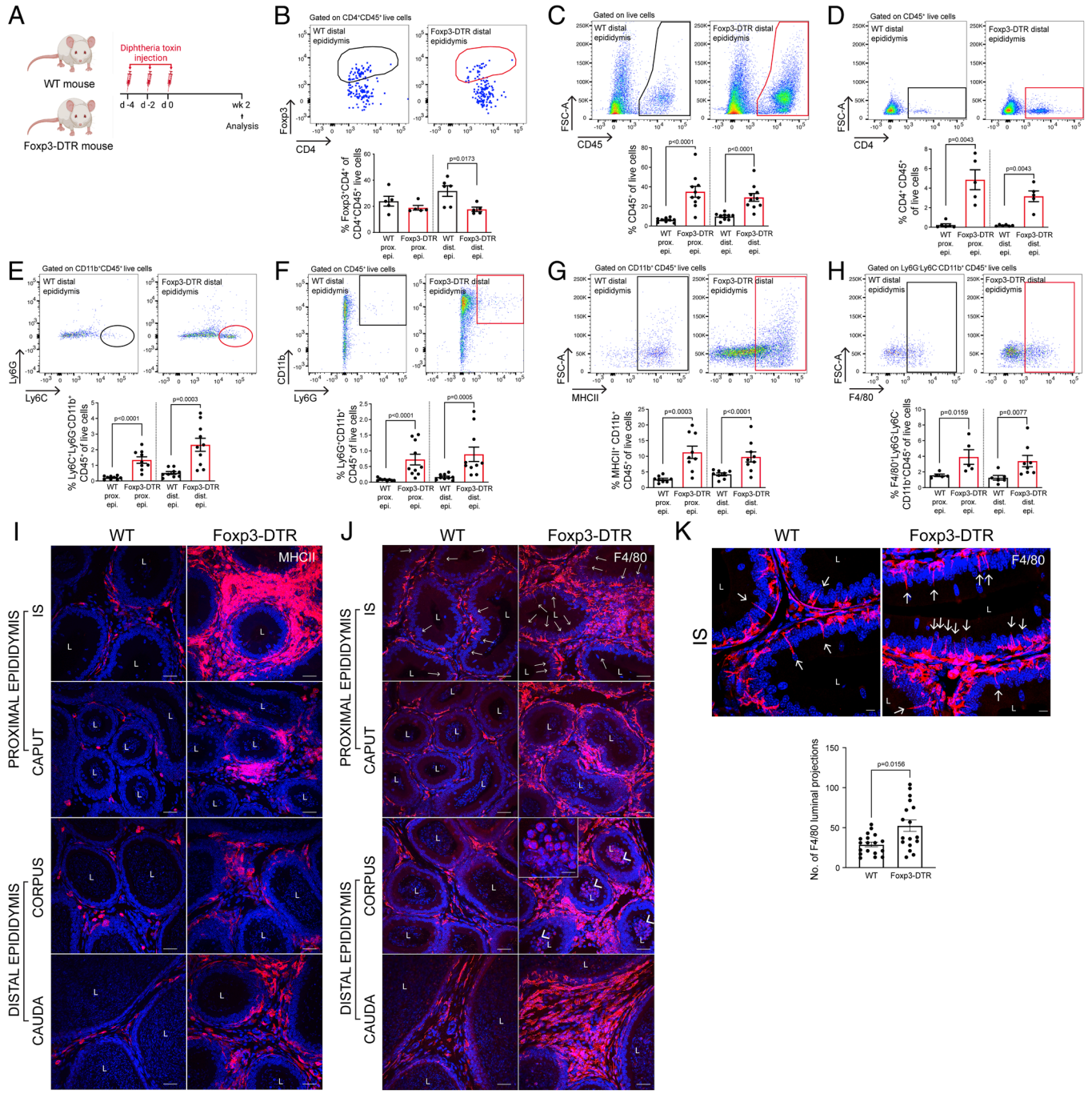

Fig. 3. Immune cell infiltration in the epididymis of Foxp3-DTR mice 2 wk after Treg depletion. (*A*) Treg cell depletion protocol and analysis 2 wk after DT treatment. Flow cytometry analysis of different immune cells in the proximal and distal epididymides of WT and Foxp3-DTR mice 2 wk after DT injections: (*B*) Tregs ($Foxp3^+CD4^+CD45^+$), (*C*) $CD45^+$ cells, (*D*) $CD4^+$ T lymphocytes ($CD4^+CD45^+$), (*E*) monocytes ($Ly6C^+Ly6G^-CD11b^+CD45^+$), (*F*) neutrophils ($Ly6G^+CD11b^+CD45^+$), (*G*) $MHCII^+$ MPs ($MHCII^+CD11b^+CD45^+$), and (*H*) $F4/80^+$ MPs ($F4/80^+Ly6G^-Ly6C^-CD11b^+CD45^+$). Note that flow cytometry dot blot analysis for distal epididymis only is shown, but quantitative data for both proximal and distal tissues are provided. Each dot represents a pool of proximal or distal regions from each mouse. Confocal microscopy images showing accumulation of (*I*) $MHCII^+$ MPs (red), (*J*) $F4/80^+$ MPs (red), and their luminal projections (arrows) in all epididymal regions of Foxp3-DTR mice after DT treatment, compared to WT. Arrowheads show infiltration of $F4/80^+$ cells within the epididymal lumen of DT-injected Foxp3-DTR mice. (*K*) Quantification of the number of F4/80 luminal projections (arrows) in the IS of DT-injected WT and Foxp3-DTR mice per area of tissue (110,000 μm^2). Each image quantification is represented as a dot. Data were analyzed using the Mann–Whitney *U* test. Data are shown as means ± SEM. Nuclei are labeled with DAPI (blue). Bars: 5 μm. L: lumen.

mice (574 proteins in proximal EVs, 92 proteins in distal EVs, and 53 proteins expressed in both proximal and distal EVs), revealing a marked alteration in the epididymal EV protein content of DT-injected Foxp3-DTR mice.

Volcano plots display the differentially expressed proteins from the proximal and distal epididymal EVs between DT-injected WT and Foxp3-DTR mice (Fig. 6*C*). We identified 40 up-regulated and 324 down-regulated proteins in the proximal epididymal EVs of Treg-depleted mice, and 36 up-regulated and 49 down-regulated proteins in the distal epididymal EVs of Treg-ablated mice (Fig. 6*C*). The complete lists of up- and down-regulated EV proteins are provided in Datasets S2–S5.

Interestingly, we found a large number of down-regulated EV proteins related to sperm maturation and epithelial function in

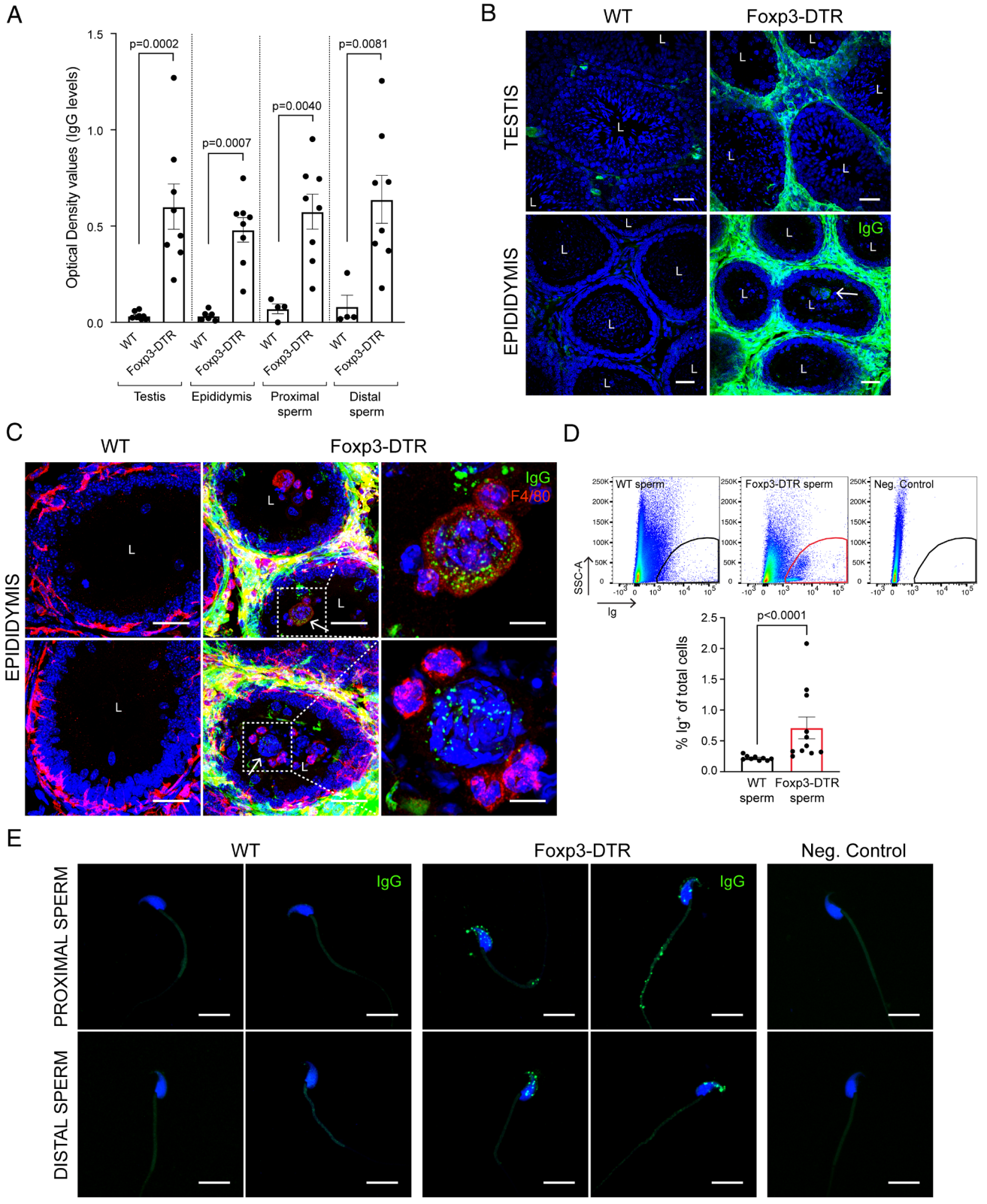

Fig. 4. Accumulation of immunoglobulin G (IgG) in Foxp3-DTR mice 2 wk after Treg depletion. (*A*) Detection of IgG against testicular, epididymal, and proximal and distal sperm antigens in the serum of DT-injected WT and Foxp3-DTR mice. (*B*) Immunolabeling of IgG (green) in the testis and epididymis of DT-injected WT and Foxp3-DTR mice. See images of other epididymal regions in *SI Appendix*, Fig. S10. Arrow shows agglutination of sperm (sperm clumping) containing anti-sperm IgG (green) in the lumen of DT-injected Foxp3-DTR mice. (*C*) Immunolabeling of F4/80$^+$ MPs (red) and IgG (green) in the epididymis of DT-injected WT and Foxp3-DTR mice. Arrows show agglutination of sperm positive for IgG (green), surrounded by F4/80$^+$ MPs (red). In the third top panel, there is apparent phagocytosis of antibody-bound sperm by MPs (red) in the DT-injected Foxp3-DTR mice. Nuclei are labeled with DAPI (blue). Bars (*B* and *C*): 20 μm, Bars (*C*, magnifications): 5 μm, L: lumen. (*D*) Flow cytometry analysis of Ig$^+$ cells (sperm) in the epididymal lumen of DT-injected WT and Foxp3-DTR mice. Each dot represents each mouse. Data were analyzed using the Mann–Whitney *U* test. Data are shown as means ± SEM. (*E*) Immunolabeling of IgG (green) in proximal and distal sperm from DT-injected WT and Foxp3-DTR mice. Nuclei are labeled with DAPI (blue). Bars: 10 μm.

the epididymal EVs of DT-injected Foxp3-DTR mice (Fig. 6 *D* and *E*). For instance, Treg-depleted EVs display reduced levels of proteins that play crucial roles in sperm motility (34–38) (*Rab5b*, *Rab11, Gpx4*, *Acly*, *Adam7*, and *Ywhae*), acrosome reaction (34, 39) (*Rab5b*, *Rab11, and Vamp3*), sperm–zona pellucida interaction (40) (*Hexb*), sperm–EV interaction (34, 41) (*Mfge8*), and some involved in signaling pathways known to regulate sperm function such as Hedgehog and Notch (42–44), Rho (45–47), Wnt (48), and MAPK (49) (Fig. 6 *D* and *E*). We also found downregulation of chaperonin-containing T-complex (TRiC) members (*Cct7* and *Cct8*) and peroxiredoxins (*Prdx5*) in Treg-ablated EVs. These proteins have been correlated with an increased percentage of poor-quality embryos (50), indicating that Treg depletion induced dysregulation of proteins involved in embryo development. Notably, Nixon et al. previously revealed that most of these proteins are present in mouse epididymal EVs (34).

Moreover, in the Treg-depleted epididymis, we observed deregulated EV proteins related to epithelial function. For example, F-actin-capping proteins (i.e., *Capza1*, *Capza2*, and *Capzb*) (Fig. 6 *D* and *E*) were up-regulated after tolerance disruption. However, most of the epithelial-related proteins were down-regulated in the Treg-depleted mice, reflecting an alteration in the epididymal function (Fig. 6 *D* and *E*), despite the apparent normal morphology. We also found upregulation of immunoglobulins (i.e., *Igh-3*, *Ighv1-50*, *Ighv5-16*, *Igkv8-28*, *Igkv19-93*, *Kv3ah*, *Kv5ac*, and *Kv5a5*) exclusively in EVs from DT-injected Foxp3-DTR mice (Fig. 6 *D* and *E*). In addition, we identified differential expression of several inflammatory response-associated and phagocytosis proteins in EVs after Treg ablation, such as *Coro1a*, *Usp14*, *Ctsc*, *Lcn2*, *Lgals1, Msn,* and *Serpina3k* (Fig. 6 *D* and *E*). The immune dysregulation caused by sperm tolerance ablation affects the epididymal EV proteomic profile and, thus, epididymal function, which may cause impaired sperm maturation and compromised sperm fertilization. Of note, the transcripts of many of the deregulated proteins in EVs of Treg-depleted mice were previously found in our RNA-seq analysis of CCs (32) (Fig. 6 *D* and *E*, highlighted in green), supporting the participation of CCs in EV secretion, sperm maturation, and immune modulation.

Impact of Treg Depletion on Epididymis Causing Impaired Male Fertility. In our working model (Fig. 7), Treg depletion leads to an exacerbated epididymal immune cell infiltration (T lymphocytes, monocytes, neutrophils, and MPs), an increase in the number of MP luminal projections, as well as MP infiltration within the epididymal lumen, resulting in severe autoimmune epididymitis. The development of autoimmunity results in the production of autoantibodies, which may aggravate the pro-inflammatory response. ASA potentially causes sperm agglutination and might lead to phagocytosis of ASA-bound sperm, which may be the reason for the observed low sperm counts and reduced sperm motility. In this inflammatory context, CCs respond by increasing the production of blebs, which might increase the secretion of EVs with CC origin (32, 51) and, therefore, participate in the immunological response (32) after tolerance disruption. Alterations in the epididymal epithelial function profoundly alter the protein composition of EVs, which compromises sperm maturation and fertilization. Taken together, the loss of immunological tolerance results in severe male subfertility.

Discussion

Immunological disorders account for ~15% of the cases of male infertility, mainly due to infections or autoimmune responses affecting the male reproductive tract (13, 52). However, the etiology of autoimmune male infertility is still poorly understood. Here, we report that the loss of tolerance, because of Treg depletion, leads to uncontrolled autoimmune responses affecting both the testis and epididymis and, ultimately, causes severe male subfertility. Our results address important knowledge gaps on the causes of male immunological infertility and the presence of ASA that lead to reproductive failure.

Although the role of immune cells in the male reproductive tract has been widely studied (11, 12, 53, 54), immunotolerance mechanisms in the reproductive organs are still poorly characterized. The male reproductive mucosa, which is constitutively exposed to commensal sperm antigens, must be carefully orchestrated, likely in part by Tregs. While previous studies have described the role of Tregs in maintaining the testicular tolerogenic environment (19, 55, 56), in the current work, we showed the presence of epididymal Tregs and demonstrated their essential role in maintaining sperm immunotolerance. Sperm populate these organs long after the establishment of systemic immune tolerance [4- to 5-wk-old male mice (57)]; hence, male reproductive function relies on immunosuppressive mechanisms. Interestingly, we described a decrease in Treg abundance in the epididymis in older individuals compared to the peri-pubertal period. This phenomenon might be necessary to develop a strong initial immunotolerance response to prevent deleterious effects against sperm as they begin to populate the

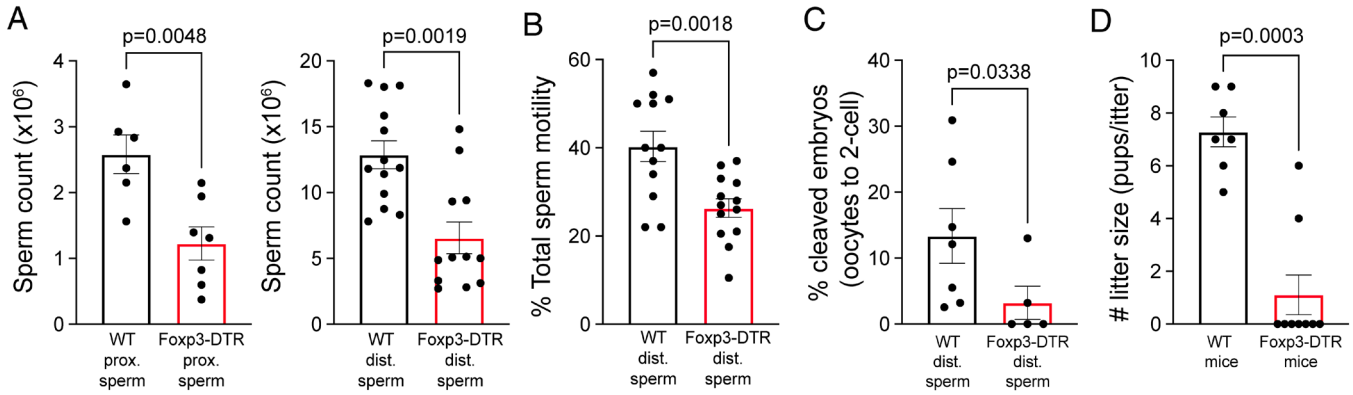

Fig. 5. Fertility assessment of Foxp3-DTR mice after Treg depletion. (*A*) Sperm count (×10^6) and (*B*) total sperm motility (%; See also Movies S1 and S2), from DT-injected WT and Foxp3-DTR mice, were assessed by CASA. (*C*) The fertilizing ability of distal sperm collected from the cauda epididymis, from WT and Foxp3-DTR mice 2 wk after DT injections, was assessed by evaluating the percentage of cleaved embryos (cleavage of oocytes to the 2-cell stage embryos). Each dot represents one sperm sample from one mouse. (*D*) Litter size (number of pups per litter) of DT-injected WT and Foxp3-DTR male mice. Each dot represents each mouse. Data were analyzed using Student's *t* test (Fig. 5*A* prox., *B*, and *C*) or Mann–Whitney *U* test (Fig. 5*A* dist. and *D*). Data are shown as means ± SEM.

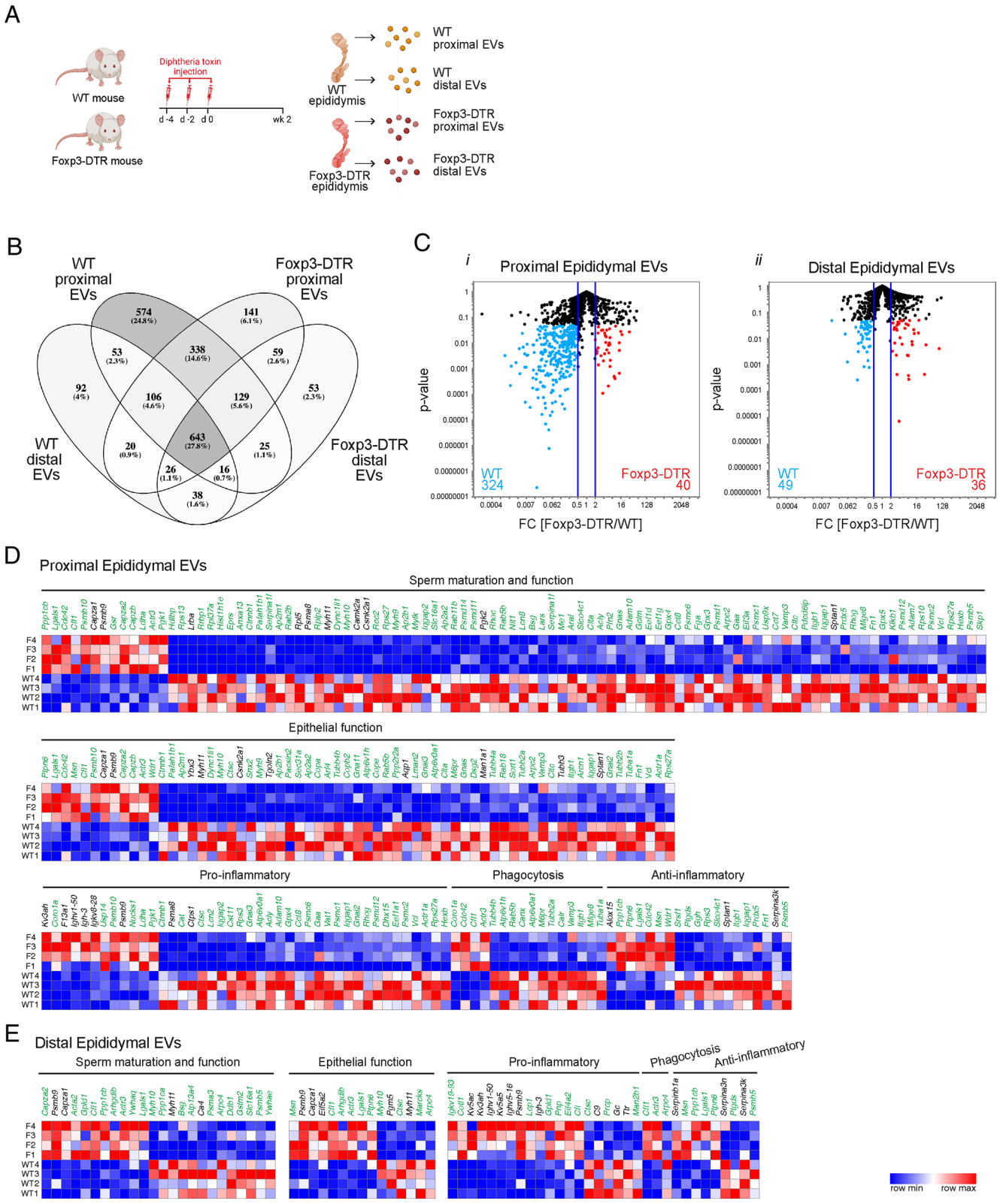

Fig. 6. Proteomic characterization of EVs from proximal and distal epididymides of DT-injected Foxp3-DTR mice. (*A*) EVs from proximal and distal epididymides were isolated from WT (n = 4) and Foxp3-DTR (n = 4) mice 2 wk after DT injections. (*B*) Venn diagram illustrating the total number (and percentage) of unique and shared identified proteins between the four EVs protein datasets (WT proximal EVs, WT distal EVs, Foxp3-DTR proximal EVs, and Foxp3-DTR distal EVs). Gray intensity correlates with protein overlapping between groups. (*C*) Volcano plot depicting the up-regulated (red) and the down-regulated (blue) EV proteins from proximal (*i*) and distal (*ii*) epididymides of DT-injected Foxp3-DTR and WT mice. Fold change (FC) ± 2; *P*-value < 0.05. The number of up- and down-regulated proteins is shown at the bottom right (red) or left (blue) sides of each graph, respectively. The blue lines show ± 2 FC. (*D*) Heat map of up- and down-regulated proteins from proximal epididymal EVs of Foxp3-DTR compared to WT mice after DT injections. (*E*) Heat map of up- and down-regulated proteins from distal epididymal EVs of Foxp3-DTR compared to WT mice after DT injections. Heat map shows proteins related to sperm maturation, epithelial function, and inflammatory factors (pro-inflammatory, phagocytosis, anti-inflammatory). Heat map represents row-normalized gene expression of the genes that encode the identified proteins using a color gradients scale ranging from higher (red) to lower (blue) relative levels. The figure displays the protein-coding genes derived from the identified deregulated proteins. Proteins whose transcripts have also been identified in CCs are highlighted in green. F: Foxp3-DTR.

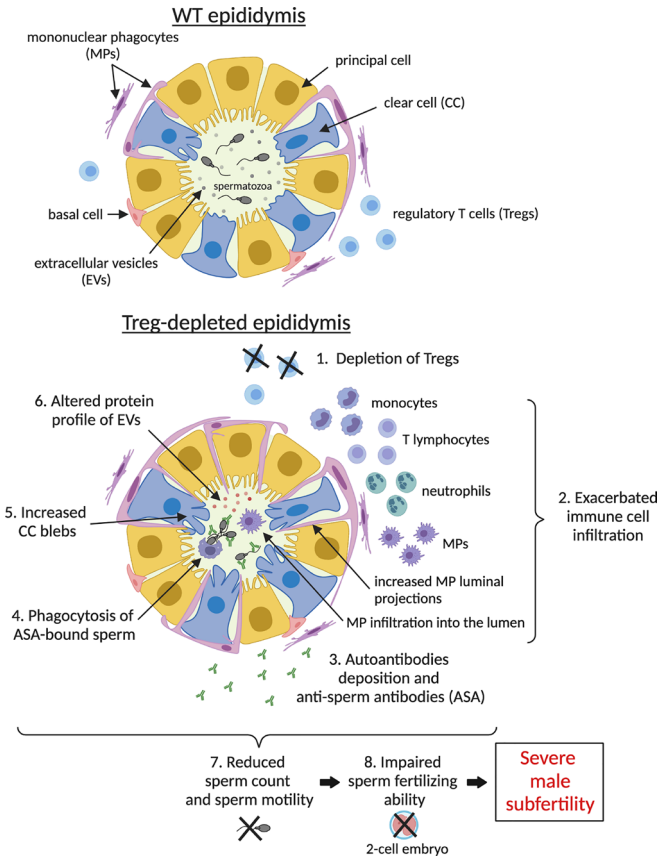

Fig. 7. Graphical representation of the key findings in Treg-depleted epididymis. The top panel represents an epididymis of a WT mouse (control). The bottom panel represents the epididymis of a Foxp3-DTR mouse 2 wk after DT treatment. The figure was created with BioRender.com.

epididymis. Intriguingly, we observe an increase in CD69$^+$ Tregs in the distal epididymis of young mice, suggesting an enhanced suppressive function of epididymal Tregs, which could contribute to preventing autoimmune responses and conserve the immune privilege milieu during puberty. In addition, during this reproductive period, there is an increase in testosterone levels that triggers spermatogenesis and sperm production (58, 59). Remarkably, testosterone, as well as other gonadal hormones, lead to differentiation and attraction of Tregs in the testis (60–63). Therefore, these increased hormone levels may also play a role in the expansion of epididymal Tregs during puberty. Interestingly, the decrease in Treg abundance during aging might have an impact on male fertility, as Treg deficiency may result in compromised sperm tolerogenic responses. This, in turn, could promote a shift toward pro-inflammatory responses, potentially inducing damage to the epididymis and testis, similar to what we observed after Treg depletion.

Although epididymal Treg abundance was still reduced 2 wk after DT, testicular Tregs rebounded, suggesting that Tregs experience a faster repopulation in the testis, similar to what has been observed in the spleen, lymph nodes, and thymus (64, 65). We detected an early infiltration of monocytes and CD4$^+$ T lymphocytes 3 d after the loss of tolerance, in both the testis and epididymis. However, the autoimmune inflammatory responses considerably aggravated 2 wk after Treg depletion, inducing severe autoimmune epididymitis and orchitis with a massive influx of F4/80$^+$ and MHCII$^+$ MPs. These first immune defenders present high phagocytic and antigen-presenting activities and release cytotoxic mediators that amplify the immune responses (66, 67). The role of MPs in the reproductive organs has been extensively studied by our group (11, 12, 68) and others (53, 54, 66) and represent one of the most abundant immune cell populations at a steady state in the epididymis (12, 66, 68–72). MPs are essential contributors to the pro-inflammatory responses after immunological tolerance ablation in other organs (73–75). Additionally, epididymal F4/80$^+$ MPs presented an increased number of luminal-reaching projections in the Treg-depleted mice. MPs project intraepithelial dendrites into the epididymal lumen compartment (11, 68, 70, 76) to sample and acquire luminal antigens (spermatozoa) (68, 70, 71). We have recently shown that the absence of CX3CR1 in MPs impairs the formation of those projections and the sampling ability (70). In our current work, when tolerance is disrupted, MPs invade the epididymal lumen, similar to what was reported in inflamed human and mouse epididymis, leading to sperm phagocytosis and oligozoospermia (77–79). Indeed, we observed engulfed sperm heads in F4/80$^+$ MPs in the epididymal lumen, suggesting that these cells may actively sense antigens located within the lumen, might sample sperm antigens, and potentially trigger an immune response toward them. Furthermore, Tung et al. showed severe autoimmune orchitis and testicular infiltration of F4/80$^+$ MPs 8 wk after Treg depletion (19). Overall, we found that the Treg ablation was followed by an aggravated inflammatory response that resulted in severe autoimmune epididymitis and orchitis.

Autoimmune diseases are characterized by the presence of autoantibodies, which are considered diagnostic markers of these disorders (80). Autoimmunity toward germ cells and sperm antigens is a cause of male infertility (10, 81). Infertile patients, as well as most vasectomized individuals, present ASA (10, 19, 81, 82). ASA are associated with reduced sperm motility and concentration and impaired sperm ability to penetrate the cervical mucus and to interact with the egg (10, 81). In our Treg depletion mouse model, we found ASA in the epididymal lumen; and those antibodies bind both the head and tail of the sperm, might cause sperm agglutination, and potentially, may lead to sperm phagocytosis (77). These defects may ultimately explain the reduced sperm counts and motility, low IVF rates, and decreased number of pups after in vivo mating observed in the Treg-depleted mice. The impaired sperm function and the presence of ASA interfere with different steps of the complex fertilization process (83) and cause the observed severe subfertility after Treg ablation. Interestingly, we found serum self-reactive antibodies against testicular, epididymal, and sperm antigens after Treg reduction. Supporting our findings, serum antibodies against testicular antigens were also reported 3 wk after Treg depletion (19).

In addition, we showed autoantibody deposition in the epididymal and testicular interstitium, which triggers and aggravates the pro-inflammatory response and leads to tissue damage (84). The accumulation of autoantibodies in the interstitium may be attributed to the protective role of the blood testicular barrier (BTB) and the blood epididymal barrier (BEB). These autoantibodies may recognize somatic antigens as well as sperm antigens, which might have been released into the interstitial space of the inflamed tissues. A similar phenomenon was previously reported following vasectomy (22). Autoantibodies might also bind to the Fc receptor of MPs in the interstitium, which lead to antibody deposition and may trigger tissue inflammation (85). Of note, we observed colocalization in the epididymal interstitium between F4/80$^+$ MPs and IgG supporting this hypothesis. However, it should be noted that the BEB does not provide the same level of protection as the BTB (86), allowing antibodies and MPs to potentially access the epididymal lumen. Importantly, it is known that under inflammatory conditions, IgG can passively cross an intact and undamaged epithelium (29). Although we did not observe any apparent damage in the epididymal epithelium, we cannot rule out the possibility of impaired integrity of the BEB, which would facilitate

the passage of both antibodies and MPs into the epididymal lumen. Moreover, evidence suggests that antibodies can enter the rete testis (87) and efferent ducts (88–90), raising the possibility that antibodies and MPs could invade the lumen of these organs and, subsequently, reach the epididymis.

Although the immune response unleashed by Treg depletion is sufficient to trigger autoimmune epididymitis and orchitis disturbing male fertility, their severity might be enhanced by the complex-mediated complement activation by antibodies (91) and by reactive oxygen species secretion from recruited immune cells (92). Overall, the present study demonstrates that ablation of immune tolerance results in severe immunological male subfertility. A similar autoimmunity-associated subfertility phenotype has been observed in Aire-deficient male mice (27, 28, 93).

During their transit through the epididymis, sperm acquire proteins and RNAs, via EVs released by epididymal epithelial cells, such as CCs and principal cells, contributing to sperm maturation (33, 34, 51, 94–98). The increased production of CC blebs as a consequence of tolerance ablation might result in an increased secretion of vesicles with CC origin (32, 51). In the Treg-depleted mice, we revealed the loss of EV-associated proteins with important roles in sperm maturation and function, sperm–egg interaction, and embryogenesis. There is evidence that the epididymal EV payload is impacted under chronic stress exposure, resulting in offspring with altered neurodevelopment (99). Also, the paternal diet influences the offspring's metabolism, probably via information trafficked from epididymis to the maturing sperm through EVs (97). Likewise, in the Treg-depleted epididymis, the strong autoinflammatory response disrupts epididymal epithelial cell function, altering the EV cargo, which may ultimately impair sperm maturation and contribute to fertility defects. The disruption of immune tolerance profoundly alters inflammatory response-associated EV composition in the epididymis. Furthermore, it is known that EVs exert a critical function in the pathogenesis of autoimmune diseases by facilitating antigen presentation and triggering inflammatory responses (100). Thus, altered EVs are contributing to the potent inflammatory responses observed in the Treg-depleted epididymis.

In summary, the loss of tolerance caused significant immune cell infiltration in the testis and epididymis, which was accompanied by a substantial deposition of autoantibodies into these tissues, ultimately affecting epididymal sperm function. The presence of ASA-bound sperm and sperm agglutination might lead to sperm phagocytosis by MPs infiltrating the epididymal lumen, which could explain the reduced sperm counts and motility, as well as the severe consequences on male fertility, in the Treg-depleted mice. Moreover, immune dysregulation strongly altered the protein composition of epididymal EVs, which reflected impaired epithelial function and compromised sperm maturation. Together, our autoimmunity-induced model might be a valuable strategy for understanding human immunological infertility with implications for infertility diagnosis and developing novel therapies to improve fertility.

Methods

Biological Material. C57BL/6-Tg(Foxp3-DTR/EGFP)23.2Spar/Mmjax (Foxp3-DTR mice) female mice and C57BL/6 WT male mice were purchased from Jackson Laboratory (Bar Harbor, ME) and bred at the Massachusetts General Hospital (MGH) animal facility to generate Foxp3-DTR or WT (control) male littermates. Foxp3-DTR transgenic mice express a diphtheria toxin receptor (DTR) fusion protein under the control of the endogenous *forkhead box P3* (*Foxp3*) promoter/enhancer regions. B1-EGFP (C57BL/CBAF1) mice express EGFP under the control of the clear cell (CC)–specific V-ATPase B1 subunit (ATP6V1B1) gene (32, 101). B1-EGFP Foxp3-DTR mice were obtained after breeding B1-EGFP mice with Foxp3-DTR mice. Four- to twenty-week-old male mice were used for all experiments. Foxp3-EGFP (C57BL6) male mice were purchased from Jackson Laboratory. CD1 IGS females were obtained from Charles River Laboratories (Wilmington, MA). The animal procedures were performed based on the NIH Guide for the Care and Use of Laboratory Animals and approved by the MGH Subcommittee on Research Animal Care.

In Vivo Depletion of Tregs. Foxp3-DTR and WT male littermates (6-wk-old) were injected (i.p) with diphtheria toxin (DT) from *Corynebacterium diphtheriae* in phosphate-buffered solution (PBS) at 40 μg/kg of body weight for Treg depletion as previously reported (19) and as described in detail in *SI Appendix*. DT-injected WT mice were used as control.

Organ Collection. Mice were anesthetized with isoflurane (2%, mixed with oxygen) and were perfused via the left cardiac ventricle with PBS as described in detail in *SI Appendix*. When tissue fixation was required, the perfusion continued with a 4% paraformaldehyde fixative.

Sperm Collection. Sperm were obtained from the proximal (IS and caput) and distal (corpus and cauda) epididymal regions of Foxp3-DTR and WT littermates after DT injections. Sperm were recovered as described in detail in *SI Appendix*.

Flow Cytometry Analysis. Proximal and distal epididymal regions and testis were mechanically dissociated by chopping followed by enzymatic digestion for 30 min at 37 °C in RPMI 1640 medium containing collagenase type I (0.5 mg/mL) and collagenase type II (0.5 mg/mL), as previously reported (68, 70). Cell suspensions were incubated for 30 min with antibodies (1:500 dilution) as described in detail in *SI Appendix*. The list of antibodies is presented in *SI Appendix* as previously reported (102).

Confocal Microscopy. The fixed organs were processed for cryosectioning and immunofluorescence, as described in detail in *SI Appendix*. The list of primary and secondary antibodies is presented in *SI Appendix* as previously reported (103, 104).

The number of F4/80$^+$ luminal projections per area of tissue (110,000 μm^2) and the number of EGFP$^+$ apical cellular protrusions (CC blebs), normalized with the number of CCs, per area of tissue (110,000 μm^2) were evaluated in epididymal sections using Fiji software.

Histological Evaluation. H&E staining was used to evaluate overall morphology as described in detail in *SI Appendix*.

ELISA. ELISA was performed as described in detail in *SI Appendix*. Blood was obtained from the left ventricle of the mouse heart, and after 30 min at room temperature (RT), samples were centrifuged at 4,000g for 10 min to obtain serum. Proteins were extracted from the testes, epididymides, and sperm of WT mice using a buffer containing 1X RIPA buffer with a protease inhibitor cocktail and a phosphatase inhibitor cocktail, as described in detail in *SI Appendix*.

CASA. Sperm were obtained as described in detail in *SI Appendix*. Sperm analysis was performed using Hamilton Thorne's CASA version 14 (Hamilton Thorne Inc.). Sperm were considered hyperactivated when presenting curvilinear velocity (VCL) ≥ 238.5 μm/s, linearity (LIN) < 33%, and amplitude of lateral head displacement (ALH) ≥ 4.22 μm, as previously reported (105). Note that total sperm motility and the analysis of capacitation-associated sperm parameters were only assessed in distal epididymal sperm.

IVF Assays. IVF assays were performed as described in detail in *SI Appendix*. Data are expressed as the percentage of cleaved embryos considering the number of 2-cell embryos over the total number of eggs inseminated.

Assessment of Fertility. Foxp3-DTR and WT male littermates (1 wk after DT injections) were individually caged with one WT female for 5 d, and mating was confirmed by the presence of a copulatory plug. The fertility assessment was calculated by the litter size (number of pups per litter).

Isolation of Epididymal EVs. Proximal and distal epididymal fluid and EVs were isolated as we previously described (51) and as described in detail in *SI Appendix*. A JEOL 1011 transmission electron microscope was used to characterize the size and shape of negatively stained EVs. A NanoSight LM10 instrument (Malvern Instruments Ltd.) with NTA software (version 3.1) was used to determine the size distribution and concentration of EVs.

Protein Extraction and Liquid Chromatography with Tandem Mass Spectrometry (LC-MS/MS) Analysis. Protein extracts were prepared as described in *SI Appendix*. Proteomic datasets of each group (n = 4) were analyzed as described in detail in *SI Appendix*.

Statistical Analysis. Data analysis was performed using GraphPad Prism version 9.4.1 (GraphPad Software; https://www.graphpad.com). To examine whether the samples were normally distributed, we performed a test of normality (Shapiro–Wilk test) and an analysis of variance [F test to compare two groups or Bartlett's test (corrected) to compare three or more groups]. Student's *t* test (two-tailed) or one-way ANOVA followed by Tukey's post hoc tests were used as parametric tests. Mann–Whitney *U* test (two-tailed) or the Kruskal–Wallis test followed by Dunn's post hoc test were used as nonparametric tests. *P*-values < 0.05 were determined statistically significant. Data were expressed as the means ± SEM. As IVF data did not accomplish the assumptions required for a parametric test, data were transformed by the arcsine(sqrt(p)) equation in which *P* is the % value/100. Once transformed, data were checked for normality and homoscedasticity, and a Student's *t* test was performed.

Ethics Approval. All animal procedures were approved by the MGH Subcommittee on Research Animal Care and were performed following the NIH Guide for the Care and Use of Laboratory Animals (National Academies Press, 2011; protocol 2003N000216).

Data, Materials, and Software Availability. The authors declare that the data supporting the findings of this study are available within supporting information files. The MS proteomics data generated have been deposited to the ProteomeXchange Consortium (http://proteomecentral.proteomexchange.org) via the PRIDE partner repository with the dataset identifier PXD041223 (106).

ACKNOWLEDGMENTS. We thank the Microscopy Core of the Program in Membrane Biology (PMB) [Massachusetts General Hospital (MGH), Boston, MA] and the MGB Molecular Imaging Core (MGH, Charlestown, MA), the Taplin Mass Spectrometry Facility (Cell Biology Department, Harvard Medical School, Boston, MA), and the HSCI-CRM Flow Cytometry Facility (MGH, Boston, MA). This work was supported by the NIH (grant HD104672-01 to M.A.B.), the MGH Sanchez Ferguson Award Faculty (to M.A.B.), the MGH Claflin Distinguished Scholar Research Award (to M.A.B.), the Lalor Foundation (to F.B. and M.L.E.), and the IBSA Foundation for Scientific Research (to F.B.). The Microscopy Core facility of the MGH PMB receives support from the Boston Area Diabetes and Endocrinology Research Center (DK57521) and the Center for the Study of Inflammatory Bowel Disease (DK43351). The Zeiss LSM 800 microscope was acquired using an NIH Shared Instrumentation Grant S10-OD-021577-01.

Author affiliations: [a]Program in Membrane Biology, Nephrology Division, Department of Medicine, Massachusetts General Hospital and Harvard Medical School, Boston, MA 02129; [b]Department of Veterinary and Animal Sciences, University of Massachusetts, Amherst, MA 01003; [c]Genetically Engineered Models Center, Whitehead Institute of Biomedical Research, Cambridge, MA 02142; and [d]Division of Immunology, Department of Microbiology and Immunobiology, Harvard Medical School, Boston, MA 02115

Author contributions: F.B., R.G.S., and M.A.B. designed research; F.B., K.O., M.L.E., M.G.G., L.J.T., D.C., and M.A.B. performed research; F.B., K.O., M.L.E., M.G.G., L.J.T., S.M., R.G.S., D.C., D.B., and M.A.B. analyzed data; and F.B., K.O., M.L.E., M.G.G., L.J.T., S.M., R.G.S., D.C., D.B., and M.A.B. wrote the paper.

1. A. McI, Mowat, Anatomical basis of tolerance and immunity to intestinal antigens. *Nat. Rev. Immunol.* **3**, 331–341 (2003).
2. D. Burzyn, C. Benoist, D. Mathis, Regulatory T cells in nonlymphoid tissues. *Nat. Immunol.* **14**, 1007–1013 (2013).
3. A. R. Muñoz-Rojas, D. Mathis, Tissue regulatory T cells: Regulatory chameleons. *Nat. Rev. Immunol.* **21**, 597–611 (2021).
4. B. R. Traxinger, L. E. Richert-Spuhler, J. M. Lund, Mucosal tissue regulatory T cells are integral in balancing immunity and tolerance at portals of antigen entry. *Mucosal Immunol.* **15**, 398–407 (2022).
5. Infertility and Fertility, US Department of Health and Human Services, National Institutes of Health. https://www.nichd.nih.gov/health/topics/infertility.
6. Infertility prevalence estimates, 1990–2021. Geneva: World Health Organization; 2023.
7. A. B. Jose-Miller, J. W. Boyden, K. A. Frey, Infertility. *Am. Fam. Physician* **75**, 849–856 (2007).
8. R. Yanagimachi, Y. Kamiguchi, K. Mikamo, F. Suzuki, H. Yanagimachi, Maturation of spermatozoa in the epididymis of the Chinese hamster. *Am. J. Anatomy* **172**, 317–330 (1985).
9. G. A. Cornwall, New insights into epididymal biology and function. *Hum. Reprod. Update* **15**, 213–227 (2009).
10. R. I. McLachlan, Basis, diagnosis and treatment of immunological infertility in men. *J. Reprod. Immunol.* **57**, 35–45 (2002).
11. N. Da Silva *et al.*, A dense network of dendritic cells populates the murine epididymis. *Reproduction* **141**, 653–663 (2011).
12. N. Da Silva, T. B. Smith, Exploring the role of mononuclear phagocytes in the epididymis. *Asian J. Androl.* **17**, 591–596 (2015).
13. M. Fijak *et al.*, Infectious, inflammatory and "autoimmune" male factor infertility: How do rodent models inform clinical practice? *Hum. Reprod. Update* **24**, 416–441 (2018).
14. A. Voisin *et al.*, Comprehensive overview of murine epididymal mononuclear phagocytes and lymphocytes: Unexpected populations arise. *J. Reprod. Immunol.* **126**, 11–17 (2018).
15. V. A. Bozhedomov *et al.*, Functional deficit of sperm and fertility impairment in men with antisperm antibodies. *J. Reprod. Immunol.* **112**, 95–101 (2015).
16. J. H. Check, Antisperm antibodies and human reproduction. *Clin. Exp. Obstet. Gynecol.* **37**, 169–174 (2010).
17. L. W. Chamley, G. N. Clarke, Antisperm antibodies and conception. *Semin. Immunopathol.* **29**, 169–184 (2007).
18. J. Kremer, S. Jager, The significance of antisperm antibodies for sperm-cervical mucus interaction. *Hum. Reprod.* **7**, 781–784 (1992).
19. K. S. K. Tung *et al.*, Egress of sperm autoantigen from seminiferous tubules maintains systemic tolerance. *J. Clin. Invest.* **127**, 1046–1060 (2017).
20. T. G. Wegmann, R. Raghupathy, Vasectomy, anti-sperm antibodies and arterial damage. *Clin. Invest. Med.* **3**, 211–212 (1980).
21. C. Rival *et al.*, Regulatory T cells and vasectomy. *J. Reprod. Immunol.* **100**, 66–75 (2013).
22. K. Wheeler *et al.*, Regulatory T cells control tolerogenic versus autoimmune response to sperm in vasectomy. *Proc. Natl. Acad. Sci. U.S.A.* **108**, 7511–7516 (2011).
23. A. Y. Rudensky, Regulatory T cells and Foxp3. *Immunol. Rev.* **241**, 260–268 (2011).
24. J. Perheentupa, APS-I/APECED: The clinical disease and therapy. *Endocrinol. Metab. Clin. North Am.* **31**, 295–320 (2002).
25. E. Kekäläinen *et al.*, A defect of regulatory T cells in patients with autoimmune polyendocrinopathy-candidiasis-ectodermal dystrophy. *J. Immunol.* **178**, 1208–15 (2007).
26. P. Ahonen, S. Myllärniemi, I. Sipilä, J. Perheentupa, Clinical variation of Autoimmune Polyendocrinopathy–Candidiasis–Ectodermal Dystrophy (APECED) in a series of 68 patients. *New Engl. J. Med.* **322**, 1829–1836 (1990).
27. F.-X. Hubert *et al.*, Aire-deficient C57BL/6 mice mimicking the common human 13-base pair deletion mutation present with only a mild autoimmune phenotype. *J. Immunol.* **182**, 3902–3918 (2009).
28. B. D. Warren *et al.*, Multiple lesions contribute to infertility in males lacking autoimmune regulator. *Am. J. Pathol.* **191**, 1592–1609 (2021).
29. V. A. Chereshnev *et al.*, Pathogenesis of autoimmune male infertility: Juxtacrine, paracrine, and endocrine dysregulation. *Pathophysiology* **28**, 471–488 (2021).
30. P. T. K. Chan, P. N. Schlegel, Inflammatory conditions of the male excurrent ductal system. Part II. *J. Androl.* **23**, 461–469 (2002).
31. C. A. Silva, M. Cocuzza, J. F. Carvalho, E. Bonfá, Diagnosis and classification of autoimmune orchitis. *Autoimmun. Rev.* **13**, 431–434 (2014).
32. M. A. Battistone *et al.*, Novel role of proton-secreting epithelial cells in sperm maturation and mucosal immunity. *J. Cell Sci.* **133**, jcs.233239 (2019).
33. R. Sullivan, Epididymosomes: A heterogeneous population of microvesicles with multiple functions in sperm maturation and storage. *Asian J. Androl.* **17**, 726–729 (2015).
34. B. Nixon *et al.*, Proteomic profiling of mouse epididymosomes reveals their contributions to post-testicular sperm maturation. *Mol. Cell Proteomics* **18**, S91–S108 (2019).
35. H. Imai *et al.*, Depletion of selenoprotein GPx4 in spermatocytes causes male infertility in mice. *J. Biol. Chem.* **284**, 32522–32532 (2009).
36. W. Zhu *et al.*, Proteomic characterization and comparison of ram (Ovis aries) and buck (Capra hircus) spermatozoa proteome using a data independent acquisition mass spectometry (DIA-MS) approach. *PLoS One* **15**, e0228656 (2020).
37. H. Choi *et al.*, Reduced fertility and altered epididymal and sperm integrity in mice lacking ADAM7. *Biol. Reprod.* **93**, 70 (2015).
38. A. Eisa *et al.*, The protein YWHAE (14-3-3 epsilon) in spermatozoa is essential for male fertility. *Andrology* **9**, 312–328 (2021).
39. P. S. Tsai, N. Garcia-Gil, T. van Haeften, B. M. Gadella, How pig sperm prepares to fertilize: Stable acrosome docking to the plasma membrane. *PLoS One* **5**, e11204 (2010).
40. P. V. Miranda, F. González-Echeverría, J. A. Blaquier, D. J. Mahuran, J. G. Tezón, Evidence for the participation of β-hexosaminidase in human sperm-zona pellucida interaction in vitro. *Mol. Hum. Reprod.* **6**, 699–706 (2000).
41. N. A. Trigg *et al.*, A novel role for milk fat globule-EGF factor 8 protein (MFGE8) in the mediation of mouse sperm–extracellular vesicle interactions. *Proteomics* **21**, e2000079 (2021).
42. T. T. Turner, H. J. Bang, S. A. Attipoe, D. S. Johnston, J. L. Tomsig, Sonic hedgehog pathway inhibition alters epididymal function as assessed by the development of sperm motility. *J. Androl.* **27**, 225–232 (2006).
43. P. Sutovsky, Sperm proteasome and fertilization. *Reproduction* **142**, 1–14 (2011).
44. D. Murta *et al.*, Notch signaling in the epididymal epithelium regulates sperm motility and is transferred at a distance within epididymosomes. *Andrology* **4**, 314–327 (2016).
45. J. S. Lee *et al.*, Actin-related protein 2/3 complex-based actin polymerization is critical for male fertility. *Andrology* **3**, 937–946 (2015).
46. C. C. Ducummon, T. Berger, Localization of the Rho GTPases and some Rho effector proteins in the sperm of several mammalian species. *Zygote* **14**, 249–257 (2006).
47. J. Kumakiri, S. Oda, K. Kinoshita, S. Miyazaki, Involvement of Rho family G protein in the cell signaling for sperm incorporation during fertilization of mouse eggs: Inhibition by Clostridium difficile toxin B. *Dev. Biol.* **260**, 522–535 (2003).
48. S. Koch, S. P. Acebron, J. Herbst, G. Hatiboglu, C. Niehrs, Post-transcriptional Wnt signaling governs epididymal sperm maturation. *Cell* **163**, 1225–1236 (2015).
49. M. W. M. Li, D. D. Mruk, C. Y. Cheng, Mitogen-activated protein kinases in male reproductive function. *Trends Mol. Med.* **15**, 159–168 (2009).

50. M. Jodar *et al.*, Sperm proteomic changes associated with early embryo quality after ICSI. *Reprod. Biomed Online* **40**, 700–710 (2020).
51. F. Barrachina *et al.*, Sperm acquire epididymis-derived proteins through epididymosomes. *Hum. Reprod.* **37**, 651–668 (2022).
52. R. Guiton, A. Voisin, J. Henry-Berger, F. Saez, J. R. Drevet, Of vessels and cells: The spatial organization of the epididymal immune system. *Andrology* **7**, 712–718 (2019).
53. A. Meinhardt, N. Dejucq-Rainsford, S. Bhushan, Testicular macrophages: Development and function in health and disease. *Trends Immunol.* **43**, 51–62 (2022).
54. S. Bhushan *et al.*, Immune cell subtypes and their function in the testis. *Front Immunol.* **11**, 583304 (2020).
55. P. Jacobo, V. A. Guazzone, C. V. Pérez, L. Lustig, CD4+ Foxp3+ regulatory T cells in autoimmune orchitis: Phenotypic and functional characterization *Am. J. Reprod. Immunol.* **73**, 109–125 (2015).
56. N. Nicolas *et al.*, Testicular activin and follistatin levels are elevated during the course of experimental autoimmune epididymo-orchitis in mice. *Sci. Rep.* **7**, 42391 (2017).
57. M. R. Bell, Comparing postnatal development of gonadal hormones and associated social behaviors in rats, mice, and humans. *Endocrinology* **159**, 2596–2613 (2018).
58. S. B. Z. Stephens, N. Chahal, N. Munaganuru, R. A. Parra, A. S. Kauffman, Estrogen stimulation of Kiss1 expression in the medial amygdala involves estrogen receptor-α but not estrogen receptor-β. *Endocrinology* **157**, 4021–4031 (2016).
59. J. Y. Wang *et al.*, Kisspeptin expression in mouse Leydig cells correlates with age. *J. Chinese Med. Assoc.* **78**, 249–257 (2015).
60. M. Fijak *et al.*, Influence of testosterone on inflammatory response in testicular cells and expression of transcription factor Foxp3 in T cells. *Am. J. Reprod. Immunol.* **74**, 12–25 (2015).
61. J. H. Lee, J. P. Lydon, C. H. Kim, Progesterone suppresses the mTOR pathway and promotes generation of induced regulatory T cells with increased stability. *Eur. J. Immunol.* **42**, 2683–2896 (2012).
62. P. Tai *et al.*, Induction of regulatory T cells by physiological level estrogen. *J. Cell Physiol.* **214**, 456–464 (2008).
63. A. Schumacher *et al.*, Human chorionic gonadotropin as a central regulator of pregnancy immune tolerance. *J. Immunol.* **190**, 2650–2658 (2013).
64. S. N. Nyström *et al.*, Transient Treg-cell depletion in adult mice results in persistent self-reactive CD4+ T-cell responses. *Eur. J. Immunol.* **44**, 3621–3631 (2014).
65. D. Watts *et al.*, Transient depletion of Foxp3+ regulatory T cells selectively promotes aggressive β cell autoimmunity in genetically susceptible DEREG mice. *Front Immunol.* **12**, 720133 (2021).
66. C. Pleuger *et al.*, The regional distribution of resident cells shapes distinct immunological immunological environments along the murine epididymis. *Elife* **11**, e82193 (2022).
67. D. A. Hume, The mononuclear phagocyte system. *Curr. Opin. Immunol.* **18**, 49–53 (2006).
68. M. A. Battistone *et al.*, Region-specific transcriptomic and functional signatures of mononuclear phagocytes in the epididymis. *Mol. Hum. Reprod.* **26**, 14–29 (2020).
69. A. C. Mendelsohn *et al.*, From initial segment to cauda: A regional characterization of mouse epididymal CD11c+ mononuclear phagocytes based on immune phenotype and function. *Am. J. Physiol. Cell Physiol.* **319**, C997–C1010 (2020).
70. F. Barrachina *et al.*, CX3CR1 deficiency leads to impairment of immune surveillance in the epididymis. *Cell Mol. Life Sci.* **80**, 15 (2022).
71. N. Da Silva, C. R. Barton, Macrophages and dendritic cells in the post-testicular environment. *Cell Tissue Res.* **363**, 97–104 (2016).
72. C. Pleuger, E. J. R. Silva, A. Pilatz, S. Bhushan, A. Meinhardt, Differential immune response to infection and acute inflammation along the epididymis. *Front. Immunol.* **11**, 599594 (2020).
73. M. Panduro, C. Benoist, D. Mathis, Treg cells limit IFN-γ production to control macrophage accrual and phenotype during skeletal muscle regeneration. *Proc. Natl. Acad. Sci. U.S.A.* **115**, E2585–E2593 (2018).
74. P. Jacobo, V. A. Guazzone, M. S. Theas, L. Lustig, Testicular autoimmunity. *Autoimmun. Rev.* **10**, 201–204 (2011).
75. C. Rival *et al.*, Functional and phenotypic characteristics of testicular macrophages in experimental autoimmune orchitis. *J. Pathol.* **215**, 108–117 (2008).
76. S. Breton, A. V. Nair, M. A. Battistone, Epithelial dynamics in the epididymis: Role in the maturation, protection, and storage of spermatozoa. *Andrology* **7**, 631–643 (2019).
77. W. Zheng *et al.*, Case report: Dendritic cells and macrophages capture sperm in chronically inflamed human epididymis. *Front. Immunol.* **12**, 629680 (2021).
78. L. Berloffa Belardin, C. Légaré, R. Sullivan, C. Belleannée, S. Breton, Expression of the pro-inflammatory P2Y14 receptor in the non-vasectomized and vasectomized human epididymis. *Andrology* **10**, 1522–1539 (2022).
79. T. E. Mullen, R. L. Kiessling, A. A. Kiessling, Tissue-specific populations of leukocytes in semen-producing organs of the normal, hemicastrated, and vasectomized mouse. *AIDS Res. Hum. Retroviruses* **19**, 235–243 (2003).
80. Z. X. Xiao, J. S. Miller, S. G. Zheng, An updated advance of autoantibodies in autoimmune diseases. *Autoimmun. Rev.* **20**, 102743 (2021).
81. A. F. Silva, J. Ramalho-Santos, S. Amaral, The impact of antisperm antibodies on human male reproductive function: An update. *Reproduction* **162**, R55–R71 (2021).
82. N. J. Alexander, D. J. Anderson, Vasectomy: Consequences of autoimmunity to sperm antigens. *Fertil Steril.* **32**, 253–260 (1979).
83. M. Kamada *et al.*, Sperm-zona pellucida interaction and immunological infertility. *Reprod. Med. Biol.* **5**, 95–104 (2006).
84. K. Fujio, T. Okamura, S. Sumitomo, K. Yamamoto, Regulatory T cell–mediated control of autoantibody-induced inflammation. *Front. Immunol.* **3**, 28 (2012).
85. R. J. Ludwig *et al.*, Mechanisms of autoantibody-induced pathology. *Front. Immunol.* **8**, 603 (2017).
86. M. P. Hedger, Immunophysiology and pathology of inflammation in the testis and epididymis. *J. Androl.* **32**, 624–640 (2011).
87. R. A. Knee, D. K. Hickey, K. W. Beagley, R. C. Jones, Transport of IgG across the blood-luminal barrier of the male reproductive tract of the rat and the effect of estradiol administration on reabsorption of fluid and IgG by the epididymal ducts. *Biol. Reprod.* **73**, 688–694 (2005).
88. K. W. Beagley, Z. L. Wu, M. Pomering, R. C. Jones, Immune responses in the epididymis: Implications for immunocontraception. *J. Reprod. Fertil. Suppl.* **53**, 235–245 (1998).
89. M. Dym, L. J. Romrell, Intraepithelial lymphocytes in the male reproductive tract of rats and rhesus monkeys. *J. Reprod. Fertil.* **42**, 1–7 (1975).
90. K. S. K. Tung, N. J. Alexander, Monocytic orchitis and aspermatogenesis in normal and vasectomized rhesus macaques (Macaca mulatta). *Am. J. Pathol.* **101**, 17–29 (1980).
91. J. M. Thurman, R. Yapa, Complement therapeutics in autoimmune disease. *Front Immunol.* **10**, 672 (2019).
92. R. J. Aitken, M. A. Baker, Oxidative stress, spermatozoa and leukocytic infiltration: Relationships forged by the opposing forces of microbial invasion and the search for perfection. *J. Reprod. Immunol.* **100**, 11–19 (2013).
93. E. Kekäläinen, N. Pöntynen, S. Meri, T. P. Arstila, H. Jarva, Autoimmunity, not a developmental defect, is the cause for subfertility of autoimmune regulator (Aire) deficient mice. *Scand J. Immunol.* **81**, 298–304 (2015).
94. U. Sharma *et al.*, Small RNAs are trafficked from the epididymis to developing mammalian sperm. *Dev. Cell* **46**, 481–494.e6 (2018).
95. W. Zhou, G. N. De Iuliis, M. D. Dun, B. Nixon, Characteristics of the epididymal luminal environment responsible for sperm maturation and storage. *Front. Endocrinol. (Lausanne)* **9**, 59 (2018).
96. R. Machtinger, L. C. Laurent, A. A. Baccarelli, Extracellular vesicles: Roles in gamete maturation, fertilization and embryo implantation. *Hum. Reprod. Update* **22**, 182–193 (2016).
97. U. Sharma *et al.*, Biogenesis and function of tRNA fragments during sperm maturation and fertilization in mammals. *Science* **1979**, 391–396 (2016).
98. E. R. James *et al.*, The role of the epididymis and the contribution of epididymosomes to mammalian reproduction. *Int. J. Mol. Sci.* **21**, E5377 (2020).
99. J. C. Chan *et al.*, Reproductive tract extracellular vesicles are sufficient to transmit intergenerational stress and program neurodevelopment. *Nat. Commun.* **11**, 1499 (2020).
100. M. Lu *et al.*, The role of extracellular vesicles in the pathogenesis and treatment of autoimmune disorders. *Front. Immunol.* **12**, 566299 (2021).
101. R. L. Miller *et al.*, V-ATPase B1-subunit promoter drives expression of EGFP in intercalated cells of kidney, clear cells of epididymis and airway cells of lung in transgenic mice. *Am. J. Physiol. Cell Physiol.* **288**, C1134–C1144 (2005).
102. R. G. Spallanzani *et al.*, Distinct immunocyte-promoting and adipocyte-generating stromal components coordinate adipose tissue immune and metabolic tenors. *Sci. Immunol.* **4**, eaaw3658 (2019).
103. T. G. Păunescu *et al.*, cAMP stimulates apical V-ATPase accumulation, microvillar elongation, and proton extrusion in kidney collecting duct A-intercalated cells. *Am. J. Physiol. Renal Physiol.* **298**, F643–F654 (2010).
104. N. Pastor-Soler *et al.*, Aquaporin 9 expression along the male reproductive tract. *Biol. Reprod.* **65**, 384–393 (2001).
105. G. Carvajal *et al.*, Impaired male fertility and abnormal epididymal epithelium differentiation in mice lacking CRISP1 and CRISP4. *Sci. Rep.* **8**, 17531 (2018).
106. Y. Perez-Riverol *et al.*, The PRIDE database resources in 2022: a hub for mass spectrometry-based proteomics evidences. *Nucleic Acids Res.* **50**, D543–D552. (2022).